Synthesis of lumped transmission-line analogs

Joshua W. Phinney
Exponent, Inc.
420 Lexington Ave., Suite 1740
New York, NY 10170
Email: jphinney@exponent.com

David J. Perreault
Massachusetts Institute of Technology
77 Massachusetts Ave., Room 10-039
Cambridge, MA 02139
Email: djperrea@mit.edu

Jeffrey H. Lang
Massachusetts Institute of Technology
77 Massachusetts Ave., Room 10-050
Cambridge, MA 02139

***Abstract*— Transmission lines and their lumped approximating networks have long been incorporated into radio-frequency power amplifiers to improve efficiency and shape circuit waveforms, and are beginning to perform a similar roles in high-frequency switched-mode power electronics. Though lumped line-simulating networks are often preferred to their distributed exemplars for reasons of design flexibility and manufacturability, the impedance peaks and nulls of such lumped networks must be aligned in a precise, harmonic manner to minimize loss and symmetrize converter waveforms. This paper addresses the issue of harmonic frequency alignment in line-simulating networks, presenting new analytic results for predicting the impedance-minimum and -maximum frequencies of networks in a ladder form. Two means of correcting for the observed harmonic misalignment in practical structures will be presented, corroborated by measurements of laminar structures built into the thickness of printed-circuit boards. These structures comprise inductances and capacitances whose dimensions are largely decoupled, such that the simulated line can be accurately analyzed and designed on a lumped basis. The presented techniques will be placed within a power-electronics setting by a representative application incorporating a lumped, line-simulating network.**

I. Introduction

The application of transmission lines to power electronics is a promising technique for miniaturizing dc-dc and dc-ac converters, and will be considered here and in a complementary paper (see [1]) at the component and converter scale. This paper will focus on component-level techniques, presenting methods for modelling and constructing networks that mimic transmission lines. Such transmission-line analogs can introduce delay into switching cells in a manner that conveniently reduces the total amount of inductance or capacitance required to realize an energy-processing function. Such a decrease in "bulk" energy storage offers unique implementation advantages, such as compatibility with available laminar construction techniques, and a shift to low-loss, air-core magnetics. Moreover, whereas reduction of high-frequency parasitics is a major preoccupation of circuit and component design, the delay networks considered in this paper *incorporate* parasitics. Tolerance for these unavoidable component resonances encourages faster switching and may further decrease a converter's energy-storage requirements.

Section II will present, as motivation for this work, the waveform-shaping and symmetrizing properties of transmission lines that are useful in tuned power circuits. Section III will consider the boundary between lumped and distributed systems for line-simulating networks in ladder form, with particular care given to the frequencies at which such networks' driving-point impedance is at a local minimum or maximum. Measurements of iterated networks — compact, laminar structures embedded in the thickness of printed-circuit boards — will demonstrate the predicted deviation of impedance-extrema frequencies from harmonic coincidence. Sections IV and V present two techniques which compensate for these deviations and achieve more accurate harmonic alignment of impedance peaks and nulls. The analytic and synthetic techniques of Sections IV and V are again verified by measurements of high-order LC structures constructed into the thickness of printed circuit boards. Section VI previews the application of transmission-line analogs to high-frequency inverters, and orients the results within the context of power-circuit miniaturization.

II. Background

Open- and short-circuited quarter-wave transmission lines have reactive driving-point impedances with harmonically related maxima and minima (see Fig. 1a, and [2, Chapter 2]). These aligned peaks and nulls — whether developed by a distributed transmission line or one of its lumped analogs — have long been utilized to shape waveforms and improve efficiency in radio-frequency power amplifiers (e.g., [3, Chaper 14] and [4]–[8]). Similar applications to the design of high-frequency switched-mode power electronics are gradually emerging [9]–[13], and can be regarded as a high-order extension of single-resonant techniques [11], [12] for reducing passive-component bulk.

The waveform-shaping behavior of a transmission-line resonator terminated in a short circuit is clarified in Fig. 1. With a length ℓ and some distributed inductance (L') and capacitance (C') per unit length, the input impedance Z_{in} of a lossless line is a transcendental function with an infinite number of j-axis poles and zeros [2]. The zeros of Z_{in} lie

1-4244-9717-7/06/$20.00

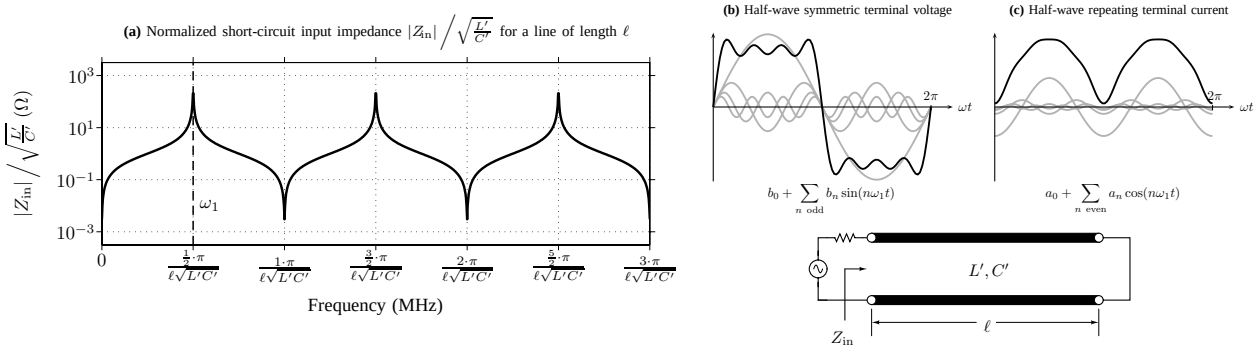

Fig. 1: **Input impedance (left) of a line of length ℓ terminated in a short circuit. When excited periodically at a frequency equal to the principle quarter-wave resonance, the line enforces odd- and even-harmonic symmetries in voltage and current, respectively.**

at $s = j\omega_\nu$, where

$$\omega_\nu = \frac{\nu\pi}{2\ell\sqrt{L'C'}} \quad \text{for } \nu = 0, 2, 4, \ldots \quad \text{and}$$

$$Z_{\rm in} = j\sqrt{\frac{L'}{C'}}\tan\left(\omega\ell\sqrt{L'C'}\right) \tag{1}$$

Impedance maxima, likewise, are located at odd multiples ($\nu = 1, 3, 5, ...$) of the principal quarter-wave resonance ω_1. Because the line will not collapse applied voltages at odd harmonics of ω_1,[1] the voltage waveform at the input port is *half-wave symmetric* for excitation periodic in $T = 2\pi/\omega_1$, as depicted in Fig. 1b. At even multiples of ω_1, the line draws large currents and the terminal current is *half-wave repeating* (*cf.* Fig. 1c) with one-half the period of the source.

Note that the V–I symmetry relations obtain even for a half-period of effort by the source. With reference to Figure 1b, consider the case of a line excited by a switch which closes from 0 to π radians of the fundamental period T. When the switch imposes a voltage waveform during the first half of the cycle, the transmission line becomes energized so as to impose a half-wave symmetric voltage at the input terminal during the second half cycle. The line stores the voltage waveform in a travelling wave along its length, which returns delayed by one-half fundamental period and inverted, because of the power-reflection condition at the short-circuit termination. The applied current wave also returns, delayed π/ω_1 seconds but not inverted, so that the line attempts to do the same work on the input network that was done on the line in the first half of the cycle.

Particular care must be given to the harmonic coincidence of the impedance peaks and nulls of line-simulating networks to preserve the waveform-symmetrizing properties of their distributed exemplars. The next three sections present methods for achieving such harmonic alignment, and clarify the boundary between lumped and distributed systems for a class of LC-ladder networks of the so-called Cauer form.[2]

III. Iterated networks

A compact approximation of a transmission delay can be constructed by cascading L-sections, as exemplified by the 3-, 4-, and 5-fold iterates of Fig. 2. In the case of such iterated, artificial lines terminated in their characteristic impedance, published bounds are available to guide a designer in selecting the order of an approximating network [14], [15, Chapter 5]. A designer can choose how many iterated L-sections, and of what electrical length, need to be concatenated for some tolerable impedance mismatch with a distributed line. No quantitative guidelines of general applicability, however, appear to have been published for *unmatched* lines, i.e., for approximating the frequencies of successive $\lambda/4$-wave resonances of artificial lines when they are terminated with an open or short circuit.[3] This unmatched case is particularly important for the filtering and symmetrizing functions of transmission lines as applied to power-electronics circuits.

To understand how minima and maxima in $Z_{\rm in}$ shift for a given degree of discretization in an iterated network with a short-circuit termination, first consider the impedances of the normalized networks of Fig. 2. As shown in the topmost network, all inductors have a value of 1 H, and all capacitors a value of 1 F.[4] The input impedances $Z_{\rm in}$ for the normalized

[1] The line is a quarter-wave transformer of the short-circuit termination at $\omega = \omega_1$, with a large impedance at that frequency and all its odd multiples. Recall that for every additional $\lambda/4$ length of line the driving-point impedance is inverted. In the lossless case the line transforms the termination from a short → open → short → ⋯ for successive zero → pole → zero → ⋯ , at each of which, successively, the line is electrically one quarter-wavelength longer.

[2] Though cascades of resonators, notably, can also simulate line impedance, we focus upon Cauer realizations because of their relative compactness beyond the $4^{\rm th}$ order [11], [12].

[3] The advice that the electrical length ℓ of component networks be shorter than a some fraction of the smallest signal wavelength of interest is often repeated [15], where "some fraction" is usually set somewhat arbitrarily as the upper bound $\ell < \lambda/10$).

[4] The impedance levels and critical frequencies of the cascaded sections can be denormalized without affecting the relative frequency relationships among poles and zeros.

$$Z_{\text{in}} = \frac{n_3}{d_3} = \frac{s^5 + 4s^3 + 3s}{s^4 + 3s^2 + 1}$$

$$Z_{\text{in}} = \frac{n_4}{d_4} = \frac{s^7 + 6s^5 + 10s^3 + 4s}{s^6 + 5s^4 + 6s^2 + 1}$$

$$Z_{\text{in}} = \frac{n_5}{d_5} = \frac{s^9 + 8s^7 + 21s^5 + 20s^3 + 5s}{s^8 + 7s^6 + 15s^4 + 10s^2 + 1}$$

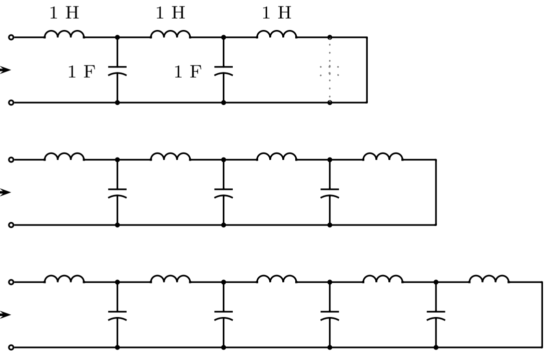

Fig. 2: **Successive diagonals of Pascal's triangle correspond to the numerator (shaded) and denominator (unshaded) coefficients of the input impedance of normalized, iterated L-networks. The k subscript of the rational impedance functions ($Z_{\text{in}} = \frac{n_k}{d_k}$) corresponds to the number of iterated L-sections. Note that the networks' short-circuit terminations effectively remove the last L-section capacitor.**

TABLE I: **Tabular arrangement of impedance-function coefficients**

d_1		1					$m=1$	$\sum_{i=1}^{1} d_{0i} = 1 \longleftarrow$ sum of coefficients in row
n_1	$n=2$	1					$m=2$	$\sum_{i=1}^{1} n_{0i} = 1$
d_2	$n=3$	1	1				$m=3$	$\sum_{i=1}^{2} d_{1i} = 2$
n_2	$n=4$	1	2				$m=4$	$\sum_{i=1}^{2} n_{1i} = 3$
d_3	$n=5$	1	3	1			$m=5$	$\sum_{i=1}^{3} d_{2i} = 5$
n_3		1	4	3			$m=6$	$\sum_{i=1}^{3} n_{2i} = 8$
d_4		1	5	6	1		$m=7$	$\sum_{i=1}^{4} d_{2i} = 13$
n_4		1	6	10	4		$m=8$	$\sum_{i=1}^{4} n_{2i} = 21$
d_5		1	7	15	10	1	$m=9$	$\sum_{i=1}^{5} d_{2i} = 34$
n_5		1	8	21	20	5	$m=10$	$\sum_{i=1}^{5} n_{4i} = 55$
		highest order	$\longleftarrow \cdots \longrightarrow$		lowest order			

1						
1	1					
1	2	1				
1	3	3	1			
1	4	6	4	1		
1	5	10	10	5	1	
1	6	15	20	15	6	1
1	7	21	35	35	21	
1	8	28	56	70		
1	9	36	84			
1	10	45				
1	11					
1						

networks are a ratio of a numerator n_k (an odd polynomial in s) and a denominator d_k (an even polynomial in s) with subscripts k equal to the number of inductors in the network.

As is evident in Table I, the numerator and denominator coefficients of n_k and d_k are diagonal sequences from Pascal's triangle (*cf.* the left-justified triangle on the right of Table I, in which the diagonals for the polynomials in $k = 3, 4$ and 5 are shown in boxes). These diagonal sequences are indexed by increasing m, beginning with $m = 1$ for the 0^{th}-order polynomial, 1, topmost in the triangle. When expressed in the staggered-order form of n_k and d_k, these polynomials are known as the Fibonacci polynomials F_m.[5] The roots of the Fibonacci polynomials are derived from hyperbolic functions in [16], though August Ferdinand Möbius expressed the roots of collapsed-order versions of the polynomials while deriving a periodicity condition for Möbius transforms [17]. The coefficients from the $m = 11$ diagonal in Table I, for instance, correspond, in Möbius' formulation, to the polynomial:

$$\sigma^5 + 9\sigma^4 + 28\sigma^3 + 35\sigma^2 + 15\sigma + 1 = 0$$

which has five roots given by

$$\sigma = -4\cos^2\left(\frac{k\pi}{m}\right) = 4\cos^2\left(\frac{k\pi}{11}\right) \qquad \text{for } k = 1, 2, \ldots, 5$$

These roots can also be expressed in terms of the roots of unity. I.e., if r denotes any m^{th} root of 1, then the corresponding root σ is $\sigma = -(1+r)^2/r$. E.g., for the 11^{th} root of unity with angle $\angle(180/11)^\circ$,

$$4\cos\left(\frac{\pi}{11}\right)^2 = \frac{[1 + 1\angle(180/11)^\circ]^2}{1\angle(180/11)^\circ} \approx 3.6825$$

Pole and zero frequencies of $Z_{\text{in}}(s)$ can be recovered from Möbius' analytic roots in σ by the substitution $\sigma = s^2 =$

[5] $F_m(x)$ evaluated at $x = 1$ yields the m^{th} Fibonacci number, as defined by the recurrence relation $F_m \equiv F_{m-2} + F_{m-1}$, where $m = 3, 4, \ldots$ and $F_1 = F_2 = 1$

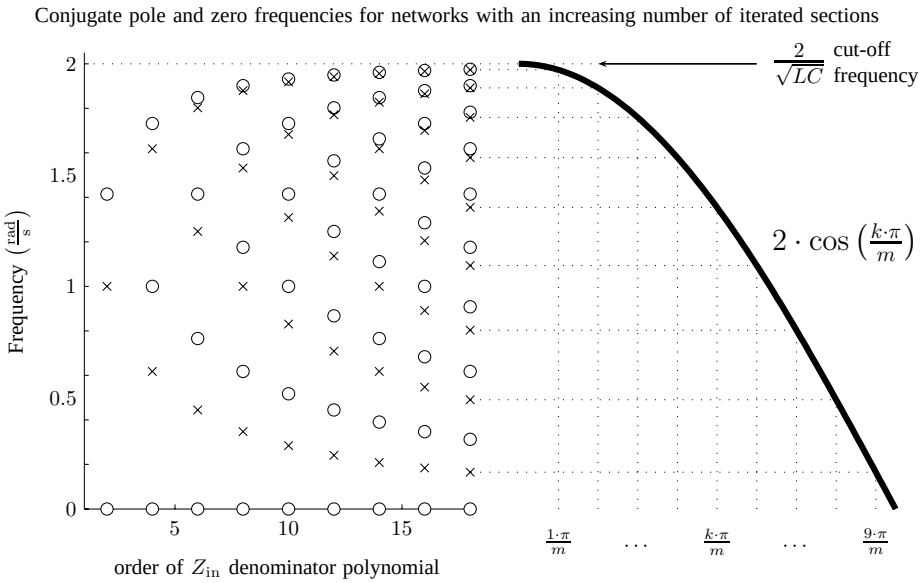

Fig. 3: **Analytical prediction of the pole and zero frequencies for iterated L-section networks, and measurements (right) of an iterated network (Section II), mutually coupled network (Section III), and Cauer-derived toroid (Section IV) built into the thickness of a printed-circuit board.**

$-\omega^2$, from which the peak frequencies ω_{p} are:

$$\omega_{\text{p}} = \sqrt{4\cos^2\left(\frac{k\pi}{m_{\text{p}}}\right)} = 2\cos\left(\frac{k\pi}{m_{\text{p}}}\right) \quad (2)$$
$$\text{for } m_{\text{p}} \text{ odd and } k = 1, \ldots, \left\lfloor \tfrac{m_{\text{p}}}{2} \right\rfloor$$

Where $\lfloor \cdot \rfloor$ is the floor function. Zero frequencies, likewise, are given by:

$$\omega_{\text{z}} = \sqrt{4\cos^2\left(\frac{k\pi}{m_{\text{z}}}\right)} = 2\cos\left(\frac{k\pi}{m_{\text{z}}}\right) \quad (3)$$
$$\text{for } m_{\text{z}} \text{ even and } k = 1, \ldots, \left\lfloor \tfrac{m_{\text{z}}-1}{2} \right\rfloor = \left\lfloor \tfrac{m_{\text{p}}}{2} \right\rfloor$$

In the Eqns. 2 and 3 above, m_p is the Pascal-diagonal m-index for the denominator (pole) polynomial, and m_z is the m-index for the numerator (zero) polynomial. Note that m_{z} is always one greater than m_{p}. These results provide analytic expressions for the pole and zero locations of uniform lumped-element transmission lines with short-circuit terminations. The impedance extrema for open-circuit terminations are given by the expressions above, after exchanging pole and zero locations appropriately.

Fig. 3a shows peak and null frequencies for increasing numbers of cascaded L-sections, demonstrating the alignment of conjugate impedance poles with the range of $2 \cdot \cos(k\pi/m)$ over $k = 1, \ldots, \lfloor m/2 \rfloor$. Critical frequencies crowd beneath the cut-off frequency, departing further from harmonic coincidence with increasing m. Impedance nulls, moreover, are never equidistant between adjacent peak frequencies as in an ideal, lossless transmission line, but are always closer to the adjacent, lower frequency pole.

A short-circuit impedance measurement of a network that approximates 28 iterated sections is shown in Fig. 4a. The frequencies of local maxima and minima in driving-point impedance are depicted by the $\times$ and $\circ$ markers in Figs. 4b, matching well with the predicted pole/zero locations[6] from Eqns. 2 and 3 (the dashed line shows the locus of analytical roots from Eqn. 2). Further details of the construction and dimensions of of this iterated network are provided in Section IV.

Whereas a transmission line terminated in an open or short is capacitive and inductive over equally broad ranges of frequency, the iterated-network Z_{in} is capacitive over an increasingly narrow band following each conjugate pole, so that the phase envelope of Fig. 4a has an inductive bias at higher frequencies. This tendency is quantified for the measured impedance of Fig. 4a by the *modal coupling* depicted in Fig. 4c. As developed in the Appendix, the coupling coefficient k is a measure of the separation between a modal frequency and the zero introduced by exciting it. The k for lumped-line modes (dashed line, Fig. 4c) can be calculated from the theoretical pole and zero frequencies of Eqns. 2 and 3, and is lower than the coupling of distributed-line modes (solid line). Measured coupling coefficients (triangle markers) for a network with 28 iterated sections closely follow the expected trend, and quantifies the uneven spacing of pole and zero frequencies observed in Fig. 4a. Methods of improving both harmonic coincidence (Fig. 4b) and coupling (Fig. 4c) to approximate the impedance of a distributed line will be considered in Sections IV and V.

[6]Fig. 3 shows all frequencies as a deviation $\Delta\omega$ from an integral multiple of the fundamental resonance ω_1, e.g., $\Delta\omega/2\omega_1$ for the first zero, and $\Delta\omega/3\omega_1$ for the 2^{nd} impedance peak.

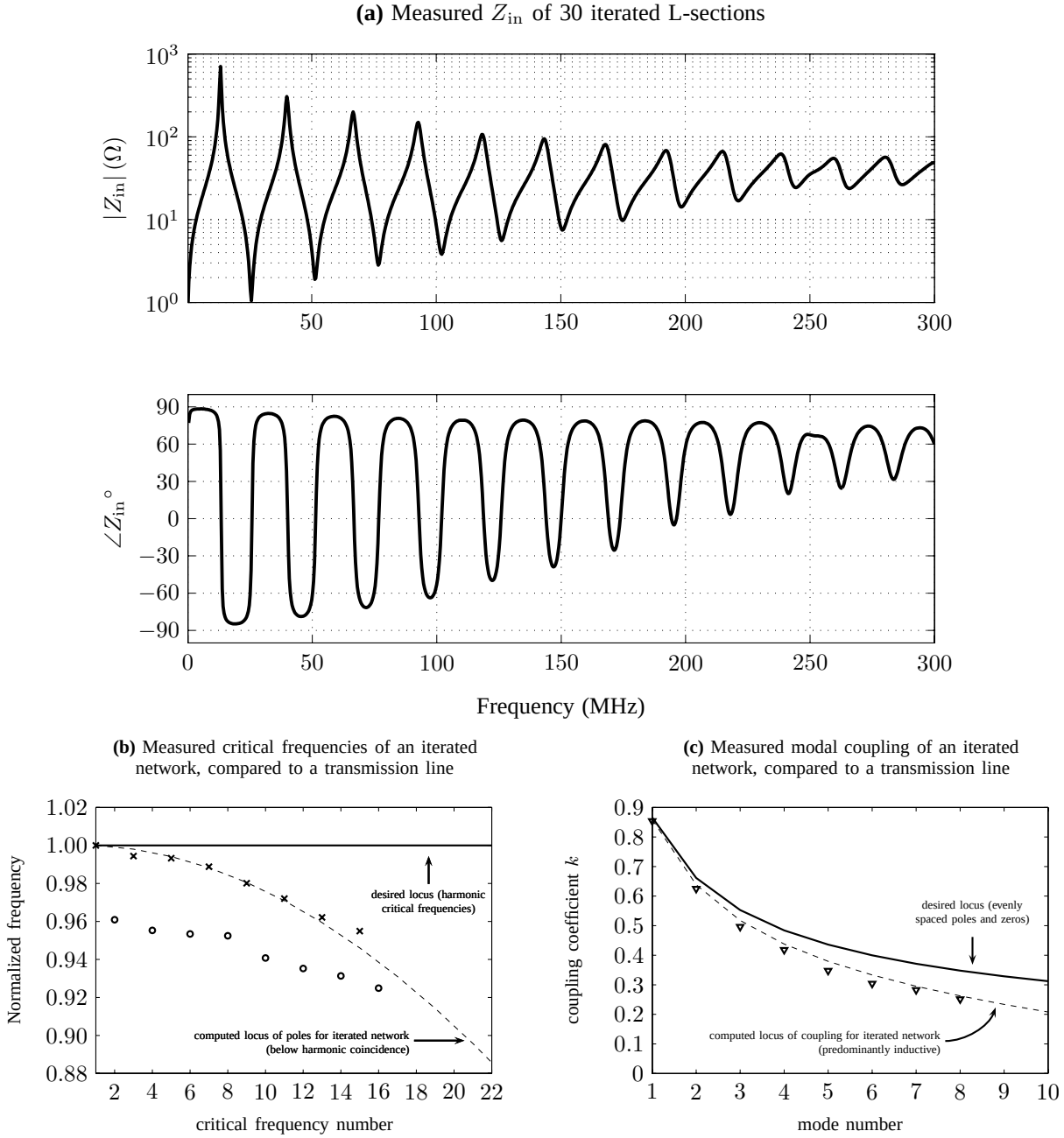

Fig. 4: **Measured input impedance of 30 iterated, coupled L-sections, showing the trend in mode coupling and the trends in pole and zero frequencies.**

IV. Iterated network with mutual inductances

The first method of compensating for the critical-frequency shortfall observed in Section III is to introduce adjacent-section mutual inductance into the iterated networks of Fig. 2. Because the calculation of mutual inductances depends on a precise specification of geometry, this section will begin by detailing the structure through which we now propose to transfer energy by both conduction current and mutual flux. This specification will provide an opportunity to discuss how the magnetically *uncoupled* measurements of Fig. 4a were made. The inductance matrices introduced in this section were calculated using FastHenry [18], a freely available program which extracts inductances and resistances of 3-dimensional conductor geometries on a quasistatic basis. The section will conclude with the impedance measurement of an magnetically coupled network, with pole and zero locations summarized in the manner of Fig. 4b.

The effect of mutual inductances will be introduced by the structure at the top of Fig. 5, from which the the impedance data of Fig. 4a were collected. The toroidal structure comprises 30 section inductances of one turn apiece (L_1–L_{30}) that are connected in series and tapped at interior nodes with 29 equal capacitances (C_1–C_{29}). The total tap capacitance

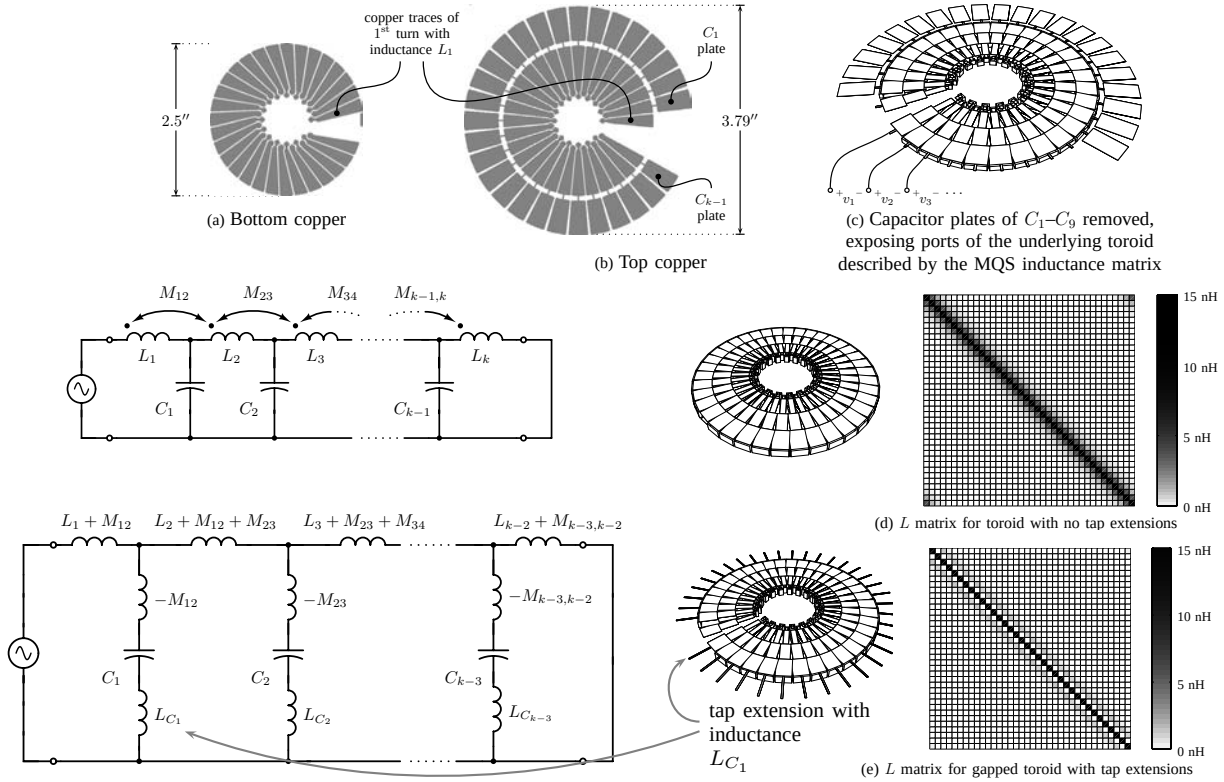

Fig. 5: **For a network with adjacent-section mutual coupling (upper schematic), Δ-Y circuit transformations reflect the mutual terms as negative inductances in the tap paths.**

is 915 pF and the total low-frequency self-inductance of the toroid is 355 nH. The structure has the dimensions shown in the top- and bottom-copper masks (reproduced in Fig. 5), and is built on two-sided 62-mil printed circuit board. A mylar film is applied over the tap-capacitor plates, with 1-mil adhesive copper foil forming the common node for the taps (a capacitance of $157.6\ \mathrm{pF/in^2}$ was measured for this method of construction). The structures was designed for a characteristic impedance of $20\ \Omega$ and a $\lambda/4$ mode at 13.56 MHz. $Z_0 = 19.7\ \Omega$ was measured, with the first quarter-wave mode at 13.41 MHz.

Though a fully populated inductance matrix would be most accurate for modelling turn-to-turn coupling in a toroid, a suitable approximation can be made by only considering *adjacent* mutual terms (*cf.* the M_{12}, M_{23}, $\ldots$,$M_{k-1,k}$ couplings in the upper schematic of Fig. 5). Because of the large flux leakage in a nonpermeable printed circuit, the mutual inductances between any two ports (where a port is two adjacent tap terminals) falls off rapidly with distance around the toroid. For the structure at the top of Fig. 5, the single-turn self-inductance is 9.97 nH.[7] The mutual inductances decrease rapidly, from 1.47 nH between adjacent turns, to 0.35 nH, 0.12 nH, ... moving clockwise or counterclockwise along the toroid. Mutual values eventually become small and negative when the turn-sections have antiparallel axes at opposite ends of the toroid.

The lower network in Fig. 5 demonstrates, by means of T-network transformations of the largest mutual terms, how inductance in tap leads offsets the mutual induction between adjacent meshes and diagonalizes the overall L-matrix. In the structure measured in Fig. 4a, 20×80-mil long inductor-traces in series with the capacitor branches cancel 1.47 nH of off-diagonal inductance to approximate the uncoupled, iterated meshes of Fig. 2. Magnetic coupling between input and output was also reduced in the measured structure by introducing a gap of 2 turns in the full toroid. The lower tableau in Fig. 5 schematically depicts the inductance matrix for this case, in which the inductances in the upper right and lower left of the L matrix have been eliminated by introducing a gap.

By shortening the length of the tap leads, a designer can offset the sub-coincident alignment of critical frequencies observed in an iterated LC network (*cf.* the dashed locus in Fig. 4b). The effect of this change in tap inductance can be explained by a frequency-dependent *cancellation* of the capacitance loading the toroid. Fig. 6a presents the measured critical frequencies of a toroid without tap extensions — but with the same dimensions and tap capacitances — as

[7] There are actually two types of turn, which extend different amounts toward the toroid's center and have slightly different self inductances. These different turns were designed for efficient packing of vias in the center rosette of the structure, so that each turn was able to accommodate 3 vias in parallel for each traverse of the board. This construction technique lowers DC and AC resistance, and was included in the analysis.

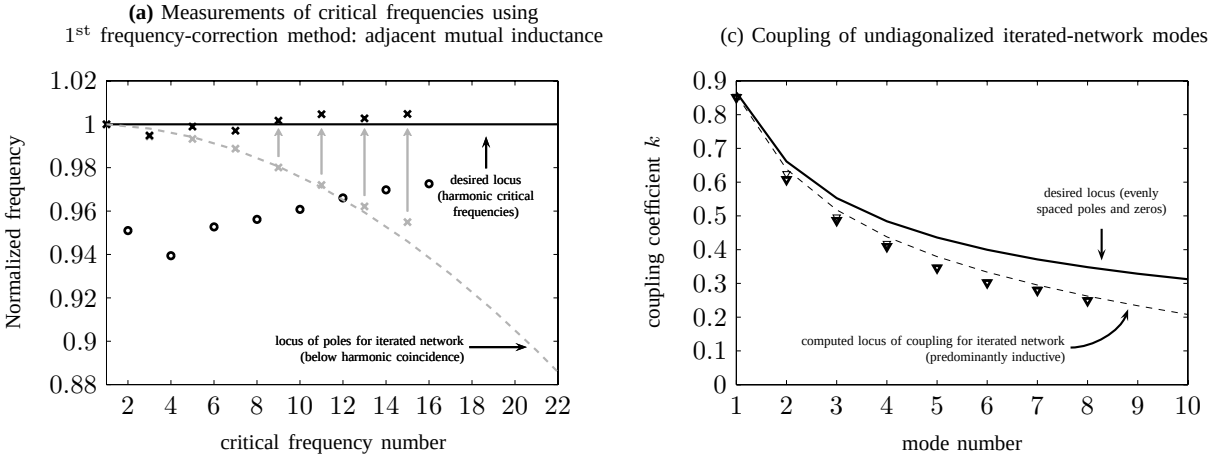

Fig. 6: **Summary of input-impedance measurement for 30 iterated, L-sections, with no tap extensions and a roughly tri-diagonal inductance matrix.**

the toroid in Section III. Compared to the diagonalized critical frequencies, which are shown in grey for comparison, the impedance peaks of the "undiagonalized" toroid are more nearly harmonic-coincident over a broader range of frequencies. The negative mutual inductance in the tap paths (-1.47 nH) is an impedance with capacitive phase that increase with frequency like an inductance. This negative inductance cancels more and more loading capacitance at higher frequencies, just compensating for the decrease in harmonic alignment expected from the iterated network. For the 20 Ω toroid measured here, the -1.5 nH tap inductance $L_{\rm t}$ is in series with $C_{\rm t} = 30.5$ pF tap capacitance. An equivalent, frequency-dependent capacitance C' for both elements is given by the series combination

$$-\frac{1}{\omega C'} = -\omega L_{\rm t} - \frac{1}{\omega C_{\rm t}} \qquad \Longrightarrow \qquad C' = \frac{C_{\rm t}}{\omega^2 L_{\rm t} C_{\rm t} + 1}$$

I.e., the effective loading capacitance has a knee frequency at $(L_{\rm t}C_{\rm t})^{-1/2}$ rad/s, beyond which it drops at 40 dB/decade. The given $L_{\rm t}$ and $C_{\rm t}$ resonate at 750 MHz, but still affect the critical frequencies by a percent or more a decade below the LC corner. The $13^{\rm th}$ critical frequency, for instance, is a pole whose modal capacitance is decreased by the factor

$$\frac{1}{1+\left(\frac{176}{750}\right)^2} = 0.947$$

corresponding to a 2.7% increase in frequency (a 3.8% change was observed). As in Section III, Impedance zeros still lie closer to the neighboring, low-frequency pole than the higher-frequency neighbor. The normalized zero frequencies are below 0.97, and the impedance-phase envelope is still inductive. Modal coupling falls below the desired transmission-line locus, and has shifted by less than $k = 0.03$ from the values in Fig. 4c.

Though capacitance offset improves harmonic alignment of higher frequencies, the alignment of the *lowest* critical frequencies is of the greatest significance for enforcing waveform symmetries. These low-frequency poles and zeros are hardly shifted by adjusting the tap inductances L_{C_1}–$L_{C_{29}}$. As with the diagonalized structure of Section III, moreover, low modal coupling prevents pole and zero frequencies from aligning *simultaneously* at harmonics of the first quarter-wave resonance.

V. Cauer-synthesized network

From the measurements presented in Figs. 4b and Fig. 6, a salient problem of iterated networks the sub-coincident alignment of zero frequencies when impedance poles are near the desired harmonic frequencies. Considered separately, the poles and zeros of iterated networks have good harmonic alignment for little design effort, less than ±1% over the first 4 critical frequencies. Incidence is poorer (about ±3% of frequency) for poles and zeros considered jointly, and a designer may need to consider more iterated LC divisions — possibly with a larger overall size — to preserve the filtering and symmetrizing functions of the lumped line.

A means of correcting the sub-coincident alignment of both poles and zeros without resorting to higher-order networks is to abandon uniform sections in favor of LC-ladder elements designed using Cauer synthesis. Cauer-derived networks preserve the basic form shown in Fig. 2, but each series-path inductor and shunt-path capacitance is specified *independently* to match the impedance of a lossless line over some desired bandwidth. The mathematics of synthesis is described elsewhere [11], [19], and synthesized L and C values are assumed to be given for purposes of this discussion.

The LC ladder values computed from Cauer synthesis can be realized with lumped inductances and capacitances to form a transmission-line approximating network. Of more interest than this straightforward approach is a technique to realize a desired Cauer network with the same family of laminar toroids used in the measurements of Sections III and IV. To implement an "integrated" Cauer network with this planar

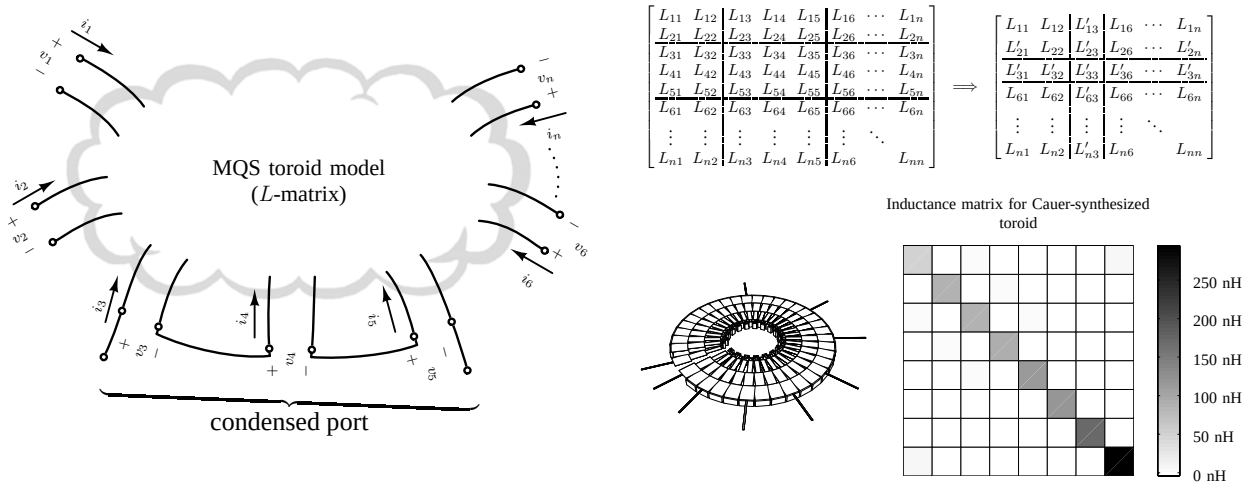

Fig. 7: **A series connection of turns condenses the inductance matrix L of the base toroid into a lower-order network of coupled inductors (8 are shown).**

construction technique, tap points can be placed around the base toroid so that the turn-inductances between taps approximate Cauer-synthesized values. Synthesized capacitances can now be added around the periphery of the toroid to complete the Cauer-derived network. The inductance matrix describing the complete turn-by-turn magnetic coupling of the toroid is related to a new, condensed inductance matrix by a the block-sum procedure depicted in Fig. 7. The new inductance matrix is described as "condensed" because the gathering of turns yields an equivalent network of lower order than the densely tapped structure depicted at the top Fig. 5.

Referring to Fig. 7, the self-inductance of a group of n turns in a series equals the appropriate $n \times n$ block sum of the full, turn-by-turn inductance matrix. The process of condensing the full L-matrix by progressive block sums is illustrated by the partitioned matrices at the top right of the figure. Primed values are self and mutual terms already condensed by summing, and the three next turns along the toroid — for this example of ladder development — are to be combined into one section inductance. The condensed self-inductance and mutual terms are

$$\text{where} \qquad L'_{33} = \sum_{i=3}^{5}\sum_{j=3}^{5} L_{ij} \tag{4}$$

$$\text{and} \qquad L''_{j3} = L''_{3j} = \sum_{i=3}^{5} L'_{ij} \qquad \text{for } j < 3$$

$$\text{and} \qquad L'_{j3} = L'_{3j} = \sum_{i=3}^{5} L_{ij} \qquad \text{for } j > 5$$

where the lower-right submatrix remains undisturbed.

The series connection of three turns shown in Fig. 7 can be expressed algebraically by noting that the gathered turns have a total voltage drop equal to the sum of three individual port voltages. The series connection introduces a transformation M between the n original port voltages v, and a new set of $n-2$ port voltages v':

$$v' = Mv = \left[\begin{array}{c:c:c} I_k & 0 & 0 \\ \hdashline 0 & 1\ 1\ 1 & 0 \\ \hdashline 0 & 0 & I_{n-k-3} \end{array}\right] \begin{bmatrix} v_1 \\ \vdots \\ v_{k+1} \\ v_{k+2} \\ v_{k+3} \\ \vdots \\ v_n \end{bmatrix} \tag{5}$$

The corresponding current transformation imposes an equality condition between connected terminals, so that $i = M^{\mathrm{T}} i'$, where i' the vector of new port currents. Under this transformation, the condensed inductance matrix L' is found by substitution to be MLM^{T}:

$$v = sLi \qquad \Longrightarrow \qquad v' = sMLM^{\mathrm{T}} i' = sL'i'$$

Though adjacent ports are shown in this example, with only one gathering of turns, the basic structure of M can be extended to any set of simultaneous connections. As one would expect form this turn-gathering procedure, the block sum of the condensed inductance matrix is identical to the block sum of the original 30×30 FastHenry matrix.

The normalized inductances and capacitances synthesized to match the first 20 non-zero critical frequencies of a lossless transmission line are shown in chart of Fig. 8.[8] The problem is to apportion toroid turns such that the new groupings have inductance-ratios that approximate the proportions in Fig. 8.

[8]Note that while C_1 is used to normalize subsequent, larger capacitances, L_2 is used as the basis for inductance normalization. L_2 is representative of the relatively constant inductance along the the artificial line's length, and L_2 and C_1 are close to the L and C values that would be necessary in an iterated ladder with the same number of meshes, and with the same $\lambda/4$ resonance. For the Cauer synthesis problem at hand, the first section inductance L_1 always approaches a value $1/2$ times as large as the second section, in the limit of many meshes. This initial half-section has a higher cutoff frequency than the full LC of the corresponding iterated line. Such half-sections appear frequently in more *ad-hoc* approximations of transmission-line impedance, *cf.* [15, Section 5.7.3].

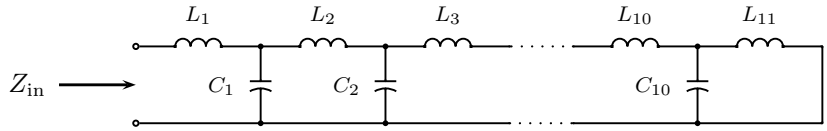

Normalized inductances				Normalized capacitances				Inductances as designed			
L_1	0.4976	L_7	1.2268	C_1	1.0000	C_7	1.2907	L'_1	11.8 nH	L'_7	26.7 nH
L_2	1.0000	L_8	1.3608	C_2	1.0097	C_8	1.4627	L'_2	26.2	L'_8	26.9
L_3	1.0147	L_9	1.5876	C_3	1.0299	C_9	1.7790	L'_3	26.7	L'_9	41.0
L_4	1.0407	L_{10}	2.0611	C_4	1.0625	C_{10}	2.6001	L'_4	26.7	L'_{10}	53.3
L_5	1.0808	L_{11}	4.0191	C_5	1.1114			L'_5	26.7	L'_{11}	104.9
L_6	1.1397			C_6	1.1831			L'_6	26.7		

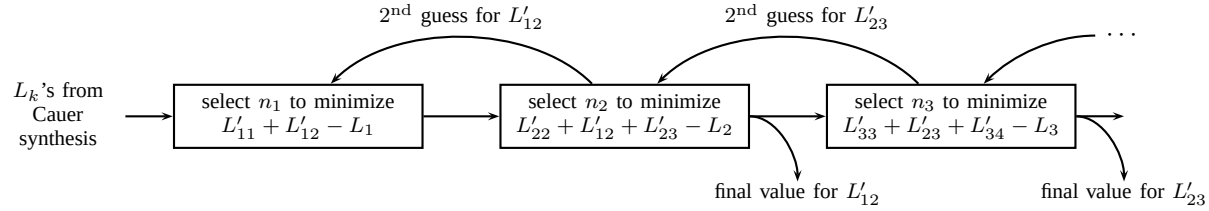

Fig. 8: **Cauer-synthesized L and C values for a 11-section ladder designed to match 21 transmission-line non-zero critical frequencies. Below, flowchart of an iterative method for determining tap locations along a toroid. The n_k are the number of turns in each Cauer-synthesized section with self-inductance L'_{kk}.**

For the 30-turn, 20 Ω toroid used in previous examples, the taps start off closely spaced at the input node, with turns per section n_k increasing counter clockwise toward the termination:

$$n_k = 1, 2\ , 2\ , 2\ , 2\ , 2\ , 2\ , 3\ , 4\ , 8 \text{ turns per section}$$

The corresponding self-inductances L_k of the condensed network likewise increase as the block-sums of 11 $n_k \times n_k$ inductance submatrices:

$$\begin{aligned} L_k \;\; = \;\; & 10.0,\ 22.1,\ 22.1,\ 22.1,\ 22.1,\ 22.1, \\ & 22.1,\ 22.1,\ 35.8,\ 48.9,\ 103.2 \text{ nH} \end{aligned}$$

The discrepancy between the sum of these self inductance (353.5 nH) and the total toroidal self inductance (355 nH measured, 366 nH calculated) is due to adjacent-section mutual entries.

As in the case of adjacent-inductor coupling discussed in Section IV, mutual inductances M in an immediate off-diagonal add to the self-inductances of the sections they couple, and appear as an impedance $-sM$ in the tap between coupled sections. These mutual terms are of the order of 10% of the tap-to-tap self-inductances, and must be taken into account for accurate pole-zero placement in the Cauer-derived toroid. Assuming that the condensed L matrix is diagonalized with tap extensions (as detailed in Section IV) we have only to consider the contribution of neighboring mutuals to any given condensed section $L'_k = L'_{kk} + L'_{k,k-1} + L'_{k,k+1}$ (i.e., the inductances as designed in Fig.V). The progressive grouping of turns along the toroid represented by Eqns. 4 and 5, however, cannot explicitly account for the mutual inductance of condensed sections yet to be designed. The iterated method summarized in Fig. V circumvents this difficulty by regrouping turns for each section k once the section $k+1$ is designed, refining the estimate of condensed section-inductance L_k' with a better approximation for the new mutual terms. The initial guess for L_k' is based upon the forward mutual inductance to a block with an identical number of turns n_k. The Cauer-derived network measured in Fig. 9 was designed using this method.

Fig. 9 shows the poles and zeros of measured impedance for a Cauer-synthesized toroid based upon the 20 Ω layout of Figure 5, with diagonalizing tap inductances and 11 condensed sections. Though poles and zeros are both in the vicinity of harmonic coincidence, their location seems much more uncertain (±3%) than in the iterated networks. The alignment of the lowest frequency poles and zeros is notably worse than the in the iterated networks (*cf.* Figs. 4b and 6), where better alignment was achieved with less design effort. Note that overall harmonic alignment (i.e., considering poles and zeros together) is not appreciably worse than in the iterated cases.

Critical-frequency alignment improves dramatically when pole and zero frequencies are compared, not to harmonically aligned values, but to the values expected after the process of turns gathering outlined previously in this Section. Because

(a) Measurements of critical frequencies using 2^{nd} frequency-correction method: Cauer synthesis

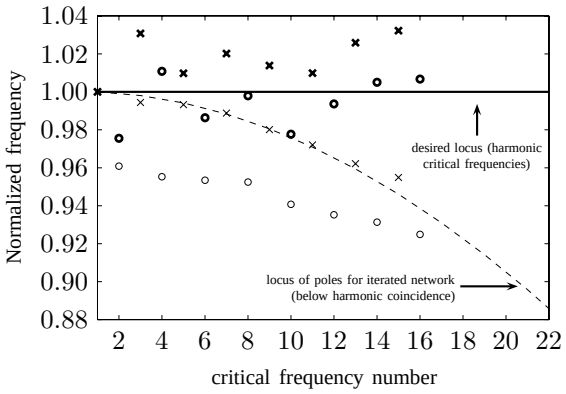

(b) Critical frequencies of Cauer network, normalized to design expectation

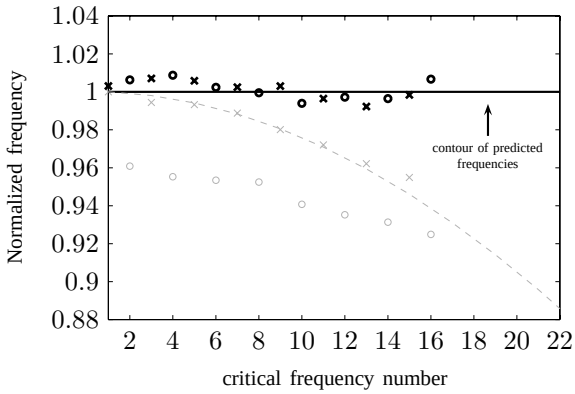

Fig. 9: **Poles and zeros of the measured impedance of a Cauer-derived toroid, based upon a 30-turn gapped toroid. In the left plot, the measured critical frequencies are normalized to the desired transmission-line locus; right, the frequencies are normalized to expectations from the synthesis model.**

of the discrete choices for section-inductance available at any given point in the network realization, the continuously increasing L and C values (typified by Fig. V) can at best be approximated. Normalizing measured poles and zeros to the frequencies computed from the approximated Cauer network yields the alignment depicted in Fig 9b: $\pm 1\%$ alignment of poles and zeros over a broad frequency range, with tighter coincidence when the first 5 or 6 critical frequencies are considered alone. This result is a strong endorsement for the accuracy of the inductance matrix computed with FastHenry. Note that stray capacitance (5 pF per tap in addition to the parallel-plate value, as layed out in copper) and lead inductance (10 nH lead inductance in series with the first section) were considered when predicting the critical frequencies for Fig 9b.

VI. Applications

Power-electronics applications of the transmission-line analogs explored in this paper are treated in an adjunct paper [1]. To place this work within a useful context, however, consider the schematic of Fig. 10, in which the dashed box around the lumped transmission line replaces the input choke of a Class E inverter. In the Introduction, it was mentioned that transmission-line techniques can reduce the total amount of inductance or capacitance required to realize an energy-processing function, which in turn can have important manufacturing benefits. For the case at hand, the Class E input choke (replaced in Fig. 10) comprises an air-core solenoid, 21 turns of 18 gauge wire, wound on a plastic former with a 26 mm diameter. Significant for manufacturability, the transmission-analog replacement is constructed directly into the thickness of a 4-layer, 2 oz. copper PCB. A 59 mil core was selected for the magnetic thickness dimension, with capacitors constructed across outer prepreg layers and an overall outer diameter of 4.4 inches. The transmission-line input network is of the iterated type analyzed in Section III, and is constructed with only 207 nH of planar inductance and about 500 pF of inter-layer capacitance. Compare these passive values with 8.02 μH inductance for the Class E design. The inverter with transmission line circulates waveforms internally to accomplish its power conversion function, exchanging large-valued blocking components for high-Q resonant elements. This tradeoff will be explored in the adjunct paper, as well as the reduced stresses attending the natural square-wave switching introduced by the transmission-line impedance (shown for an previously published case in Fig. 10).

VII. Conclusion

This paper has considered critical-frequency alignment (see Table II) of iterated and Cauer-derived transmission-line analogs with planar, air-core magnetics. For the iterated network of Sections III and IV, a relation between the critical frequencies of cascaded LC sections and the roots of Fibonacci polynomials has been presented. This result quantifies the transition between a distributed line and its lumped ladder approximations, and appears to be new in the literature. The Cauer-derived line-simulating network, with non-uniform placement of taps in approximation of the L and C values calculated by Cauer synthesis, exhibited critical frequencies matching the lumped-model prediction within $\pm 1\%$. Though the Cauer-derived network had poorer harmonic coincidence that the iterated networks, the precision of the MQS model allows this shortfall to be overcome by design. Moreover, since the Cauer network realizes a *specified* driving-point reactance, it alone — of the three options presented — permits the simultaneous harmonic alignment of *poles and zeros* necessary for the symmetrizing function of transmission networks.

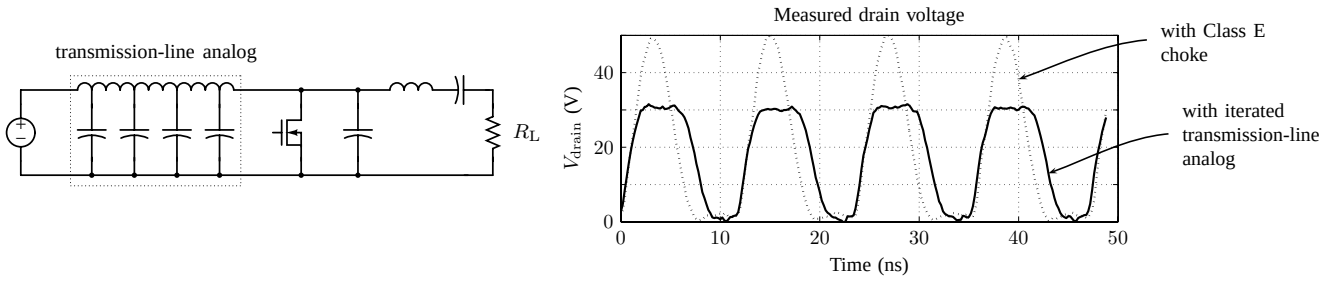

Fig. 10: **Comparison of drain-voltage waveforms for a 82 MHz class-E inverter with an inverter incorporating a transmission-line analog (a so-called Class Φ inverter).**

TABLE II: **Summary of synthesis methods for transmission-line analogs**

Structure	**Harmonic alignment**	**Coupling**	**Tolerance**
Iterated	pole and zero frequencies decrease as $\cos\left(\frac{2k}{m}\right)$	lower at high frequencies	$\pm 3.0\%$ to the 5^{th} pole; $\pm 1\%$ poles alone
Tri-diagonal	harmonic pole or zero alignment	lower at high frequencies	$\pm 2.4\%$ to the 5^{th} pole; $\pm 1\%$ poles alone
Cauer	harmonic pole and zero alignment	more even pole-zero spacing	$\pm 3.0\%$, or $\pm 1\%$ within prediction, poles+zeros

APPENDIX

Whenever driving effort excites some mode, whether native to the energy-domain of excitation or not, the coupling coefficient k represents the extent of energy conversion, and is defined over a cycle as

$$k^2 = \frac{\left(\begin{array}{c}\text{energy delivered}\\ \text{to load}\end{array}\right) + \left(\begin{array}{c}\text{energy stored and}\\ \text{recovered from load}\end{array}\right)}{\text{total energy delivered}}$$

Consider a simple case of energy storage shown in Fig. 11a: a mass slides on a frictionless plane, and is tied to a mechanical ground through a spring k_1. A force with infinite authority — i.e., no source impedance — stretches k_1 and stores energy in it. All of the energy delivered from the source stretches the spring, and the drive is perfectly coupled to k_1. For this case of zero source impedance, the coupling coefficient $k \equiv 1$.

Mode excitation is rarely as simple as the case pictured in Fig. 11a. Usually, energy stored in k_1 requires that some energy be delivered to the exciting structure, as shown in Fig. 11b. At frequencies far below resonance, the oscillator is compliance-dominated (i.e., the energy stored in m is negligible) and F stores energy in k_1 by stretching k_2. If k_2 is stiff, F is strongly coupled to k_1; if k_2 is compliant, it is stretched considerably, k_1 is relatively undisturbed, and the coupling is weak. k^2 in this case can be expressed as the fraction of total energy delivered to k_1:

$$k^2 = \frac{\text{energy stored in } k_1}{\text{energy stored in } k_1 + \text{energy stored in } k_2}$$

In laboratory practice, the frequency separation between resonance and antiresonance (i.e., between a modal resonance and the zero introduced by exciting it) is a measure of the degree of energy coupling. To understand this useful relationship, consider the impedance of Fig. 12a for the

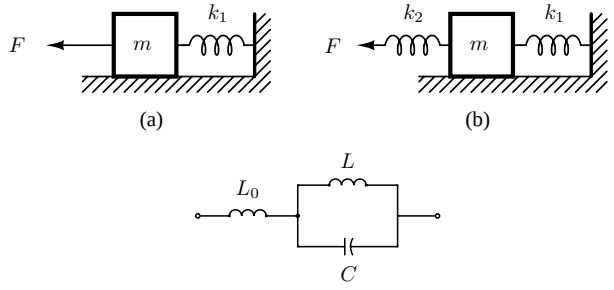

(c) Electrical analog of (b)

Fig. 11: **A simple example of coupling**

Impedance of network in Fig. 11c

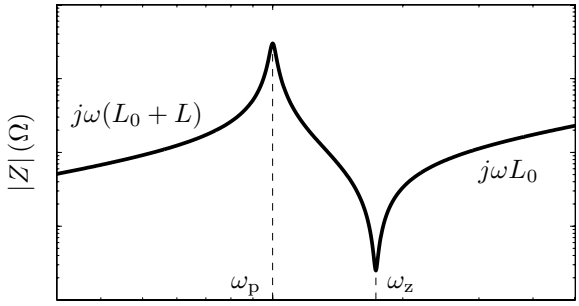

Fig. 12: **Explanation of coupling in terms of pole/zero separation**

network in Fig. 11c:

$$Z = j\omega L_0 - \frac{j}{\omega C - \frac{1}{\omega L}} = j\omega\left[L_o - \frac{L}{\omega^2 LC - 1}\right] = j\omega \cdot \frac{\omega^2 L_0 LC - L_0 - L}{\omega^2 LC - 1}$$

ω_p and ω_z from Fig. 12a are found by setting numerator and denominator to zero and solving for frequency, from which:

$$\omega_\mathrm{p} = \sqrt{\frac{1}{LC}} \quad \text{and} \quad \omega_\mathrm{z} = \sqrt{\frac{1}{L_0 \| L \cdot C}} = \sqrt{\frac{1}{LC} + \frac{1}{L_0 C}}$$

The ratio $\omega_\mathrm{z}^2/\omega_\mathrm{p}^2$ bears a useful relationship to k^2, and can be expressed as

$$\frac{\omega_\mathrm{z}^2}{\omega_\mathrm{p}^2} = \frac{L + L_0}{L_0} \quad \text{since} \quad \frac{\omega_\mathrm{z}^2}{\omega_\mathrm{p}^2} - 1 = \frac{L}{L_0}$$

By the energy definition of coupling coefficient, and for some applied current i in the low-frequency, inductance-dominated regime,

$$k^2 = \frac{\frac{1}{2}Li^2}{\frac{1}{2}Li^2 + \frac{1}{2}L_0 i^2} = \frac{L}{L_0 + L}$$

which can in turn be related to the ratio $\omega_\mathrm{z}^2/\omega_\mathrm{p}^2$:

$$1 - k^2 = \frac{L_0}{L + L_0} \quad \Longrightarrow \quad k^2 = 1 - \frac{\omega_\mathrm{p}^2}{\omega_\mathrm{z}^2} \qquad (6)$$

Using the gross pole-zero coincidence approximation $\omega_\mathrm{z} + \omega_\mathrm{p} \approx 2\omega_\mathrm{z}$,

$$k^2 = \frac{(\omega_\mathrm{z} + \omega_\mathrm{p})(\omega_\mathrm{z} - \omega_\mathrm{p})}{\omega_\mathrm{z}^2} \approx 2 \cdot \frac{\omega_\mathrm{z} - \omega_\mathrm{p}}{\omega_\mathrm{z}} \qquad (7)$$

While Eqn. 6 precisely determines k from measured ω_z and ω_p, Eqn. 7 affords the insight that pole-zero spacing increases linearly with increasing k, to a better approximation as $\omega_\mathrm{z} - \omega_\mathrm{p}$ is small with respect to either critical frequency. We can apply this single-resonant treatment of coupling to cascaded oscillators, as long as we can ignore the impedances of neighboring intertia- or compliance-dominated resonators, excited away from their tuned frequencies. This approximation, and the others of this section, are common practice within the transducer field [20, Section 4.8], and are a convenient means of comparing the alignment of adjacent poles and zeros.

REFERENCES

[1] J. Phinney, D. Perreault, and J. Lang, "Radio-frequency inverters with a transmission-line input networks," in *PESC 2006*, to appear, June 2006.

[2] D. Pozar, *Microwave Engineering*, 2nd ed. New York: John Wiley & Sons, 1998.

[3] F. Raab, *Solid State Engineering*. Atlanta: Noble, 2001.

[4] V. Tyler, "A new high-efficiency high-power amplifier," *The Marconi Review*, vol. 21, no. 130, pp. 96–109, Fall 1958.

[5] F. Raab, "Class-F power amplifiers with maximally flat waveforms," *IEEE Transactions on Microwave Theory and Techniques*, vol. 45, no. 11, pp. 2007–2012, November 1997.

[6] K. Honjo, "A simple circuit synthesis method for microwave Class-F ultra-high-efficiency amplifiers with reactance-compensation circuits," *Solid State Electronics*, vol. 44, pp. 1477–1482, 2000.

[7] F. Raab, "Maximum efficiency and output of Class-F power amplifiers," *IEEE Transactions on Microwave Theory and Techniques*, vol. 49, no. 6, pp. 1162–1166, June 2001.

[8] F. Lepine, A. Adahl, and H. Zirath, "L-Band LDMOS power amplifers based on an inverse Class-F architecture," *IEEE Transactions on Microwave Theory and Techniques*, vol. 53, no. 6, pp. 2207–2012, June 2005.

[9] R. Gutmann and J. Borrego, "Power combining in an array of microwave power rectifiers," *IEEE Transactions on Microwave Theory and Techniques*, vol. MIT-27, no. 12, pp. 958–967, December 1979.

[10] Y. Han, O. Leitermann, D. A. Jackson, J. M. Rivas, and D. J. Perreault, "Resistance compression networks for resonant power conversion," in *IEEE 36th Annual Power Electronics Specialists Conference Proceedings*, June 2005, pp. 1282–1292.

[11] J. Phinney and D. Perreault, "Filters with active tuning for power electronics," *IEEE Power Electronics Specialists Conference*, pp. 363–370, June 2001.

[12] ——, "Filters with active tuning for power electronics," *IEEE Trans. Power Electron.*, vol. 18, no. 2, pp. 636–647, March 2003.

[13] J. Phinney, "Multi-resonant passive components for power conversion," Ph.D. Thesis, Dept. of Electrical Engineering and Comp. Science, Massachusetts Institute of Technology, Laboratory for Electromagnetic and Electronic Systems, 2001.

[14] E. Guillemin, *Communication Networks, Volume II: the Classical Theory of Long Lines, Filters and Related Networks*. New York: John Wiley & Sons, 1935.

[15] T. Lee, *Design of CMOS Radio-Frequency Integrated Circuits*. Cambridge, United Kingdom: Cambridge University Press, 1998.

[16] V. Hoggatt, Jr. and M. Bicknell, "Roots of fibonacci polynomials," *The Fibonacci Quarterly*, vol. 11, no. 3, pp. 271–274, October 1973.

[17] K. Brown, "Polynomials from Pascal's Triangle," `http://www.mathpages.com/ home/kmath304.htm`, site accessed as of April 28, 2005.

[18] M. Kamon, M. Tsuk, and J.White, "Fasthenry, a multipole-accelerated preconditioned iterative methods for three-dimensional potential problems," in *Proceedings of the* 30th *Design Automation Conference*, June 1993, FastHenry is freely available for academic or commercial use; documentation and code can be downloaded from `http://www.fastfieldsolvers.com/`, last accessed May 9, 2005.

[19] E. Guillemin, *Synthesis of passive networks: theory of methods appropriate to the realization and approximation problems*. New York: John Wiley & Sons, 1957.

[20] T. Hueter and R. Bolt, *Sonics: Techniques for the use of sound and unltrasound in engineering and science*. New York: John Wiley & Sons, 1955.